Article:
Liu, H. orcid.org/0009-0005-2000-9859, Peng, N. orcid.org/0009-0001-8836-0398, Meng, W. orcid.org/0000-0003-0209-8753 et al. (3 more authors) (2024) Optical Fiber Temperature Sensing Probe based on F-P Cavity for Human Body Temperature Monitoring. IEEE Sensors Journal. ISSN 1530-437X

https://doi.org/10.1109/jsen.2024.3385203

Optical Fiber Temperature Sensing Probe based on F-P Cavity for Human Body Temperature Monitoring

Haojie Liu, Nian Peng, Wei Meng, *Member, IEEE*, Zude Zhou, Quan Liu, *Member, IEEE*, and Shane Xie, *Fellow, IEEE*

***Abstract*—In the exoskeleton-assisted rehabilitation scenarios, sensors need to have strong resistance to environmental interference and long-term monitoring stability. Commonly used body temperature measurement equipment cannot be recorded and worn for long periods. Based on the advantages of optical fiber sensors that are resistant to electromagnetic interference, have strong environmental adaptability, and have good stability after being fabricated and packaged in a specific structure. This article proposes a human body temperature sensing probe that uses capillary copper tubes to encapsulate the F-P cavity structure. The UV glue is applied at the end of the optical fiber and cured to form an F-P microcavity, which is encapsulated with a copper tube for thermal conductivity and protection. It can be fixed anywhere on the body surface with medical tape. Theoretical derivation and numerical simulation are carried out on the interference principle and temperature sensing principle of the F-P cavity. The characteristics of the sensing probe are tested and body temperature monitoring is performed on the human wrist and armpit. The experimental results show that the probe has good stability, repeatability, sensitivity and signal-to-noise ratio. The average standard deviation of the dip wavelength at constant temperature is 16.7 pm. The sensor sensitivity is about 287.3 $pm/^\circ\mathrm{C}$. The capillary structure makes the temperature response speed faster than that of electronic sensors. The proposed F-P sensing probe can be applied to human body sign information monitoring and feedback in rehabilitation, which is conducive to the realization of efficient and intelligent rehabilitation strategies.**

***Index Terms*—Optical fiber sensor, F-P cavity, body temperature monitoring.**

I. Introduction

ACCORDING to the "World Population Prospects 2022" report released by the United Nations on July 11, it is expected that the elderly population aged 60 and above will exceed 500 million in 2050 [1], and China will enter a severely aging society. The growth of the elderly population has led to an increase in the rate of stroke patients. Additionally, the number of hemiplegia patients caused by traffic accidents is also increasing yearly. Rehabilitation training is crucial for the limb recovery of these groups of people. A rehabilitation assistance robot is an indispensable equipment that can help patients with physical disabilities restore their limb movement [2]. The perception of physiological parameters is conducive to real-time feedback of the human body's physical condition to the rehabilitation assistance equipment and helps to optimize the rehabilitation training plan. Body temperature, as one of the physiological parameters, can reflect changes in body surface temperature in local training areas and human body core temperature, and human body core temperature is closely related to human metabolism and fatigue [3]. Comprehensive analysis of human body temperature and other physiological information is of great clinical significance, which can timely adjust of the robot's working parameters and improve rehabilitation efficiency.

Commonly used sensors for measuring body temperature are mainly digital thermometers, infrared thermometers, and mercury thermometers. They are accurate, safe, convenient, and easy to use. However, they are not wearable and cannot continuously monitor body temperature for a long time. Therefore, an increasing number of researchers have developed electronic skin temperature sensors based on micro-machining technology and advanced sensing substrates. These sensors have high sensitivity, high resolution, fast response, and high repeatability, but the complex process and material cost make them not cost-effective [4]. Optical fibers are made of high-performance polymers, high-purity glass, quartz and other materials. These materials have high impedance to electromagnetic waves. The structural design of the optical fiber sensor gives it good protection performance, which can reduce the impact of electromagnetic interference on the sensor. Moreover, light waves propagate through total reflection in optical fibers and propagate very fast. Therefore, optical fiber has strong anti-interference ability. The material and structure of the optical fiber sensor can provide certain protection and corrosion resistance, and can adapt to extreme environments. Based on its strong anti-electromagnetic interference and environmental adaptability, it has been widely used in fields such as engineering structural health monitoring [5], environmental monitoring [6], safety protection [7], and medical care [8]. Using new materials and optimized structural design, optical fiber sensors with high tensile properties have been used for human physiological and behavioral information monitoring and intelligent pronunciation recognition [9], [10]. Especially in exoskeleton rehabilitation scenarios, the activation of elec-

This work was supported by the National Natural Science Foundation of China under Grant 52275029 and Grant 52075398. (Corresponding authors: Nian Peng, Wei Meng)

Haojie Liu, Nian Peng, Wei Meng and Quan Liu are with the School of Information Engineering, Wuhan University of Technology, Wuhan, 430070, China (e-mail: nianpeng@whut.edu.cn; weimeng@whut.edu.cn).

Zude Zhou is with the School of Mechanical and Electronic Engineering, Wuhan University of Technology, Wuhan, 430070, China.

Shane Xie is with the School of Electronic and Electrical Engineering, University of Leeds, Leeds LS2 9JT, United Kingdom.

tric actuators will cause interference in the electrical sensing system [11]. As an excellent candidate, optical fiber sensors can realize synchronize monitoring of limb movements and physiological states during patient rehabilitation training, and provides effective feedback information for the formulation of personalized rehabilitation plans and intelligent rehabilitation assessment [12].

Based on different optical principles, structural designs, and packaging methods, they are easy to make into physiological sensors that can be worn on the human body. Moreno et al. [13] have mentioned that microclimate variables between wearable robots and human limbs are important parameters to improve user comfort and minimize the risk of injury. Microclimate variables include temperature and relative humidity. Since the temperature sensitivity coefficient of the single mode FBG sensor is only 10.8 $pm/\,^{\circ}\mathrm{C}$ [14]. Leal-Junior et al. [15] increased the sensor's sensitivity by embedding FBG into TPU and PLA printing materials. They also took advantage of the higher flexibility and fracture toughness and better biocompatibility of polymer optical fibers to propose a system that can measure microclimate temperature and relative humidity [16]. The sensitivity of the optical fiber sensor based on the F-P interference principle is higher than that of the wavelength modulated sensor. Liu [17] produced a dual-parameter optical fiber sensor based on a cascade of fiber Bragg grating and Fabry-Perot interferometer (FPI) structures, which has high temperature and air pressure sensitivity. Wang [18] also proposed a system for measuring temperature and humidity simultaneously using similar FBG and F-P interference structures. Reference [19] reported a high-resolution optical fiber temperature sensor system based on a air-filled F-P cavity. Liang [20] proposed an ultrasensitive (11.93 $nm/\,^{\circ}\mathrm{C}$) temperature sensor based on enhanced vernier effect. The aforementioned temperature sensors, utilizing F-P cavities, are finely crafted and possess outstanding sensitivity. Mostly used for high temperature monitoring of the environment.

Based on the interference structure of the F-P cavity, this paper proposes a packaging method that can quickly conduct heat and protect the F-P microcavity structure, which is convenient for human body measurement. The sensing probe is simple to manufacture and low in cost. Through experimental analysis, it has fast response, good repeatability, high sensitivity, good signal-to-noise ratio (SNR), and is easy to be placed on any part of the body. The rest of this paper is organized as follows. Section II introduces the sensing principle, numerical simulation, and fabrication of the F-P microcavity sensing probe. Section III is experiments and discussions, and Section IV is the conclusion.

II. Sensor Principle and Fabrication

A. F-P Cavity Interference Principle

The F-P cavity structure produced in this paper is formed by curing UV glue at the end of the optical fiber. Its working principle is shown in Fig.1. The incident light is reflected on the optical fiber-UV glue and UV glue-air surfaces respectively. The reflectivity R_1 and R_2 of the two reflecting surfaces can be expressed as:

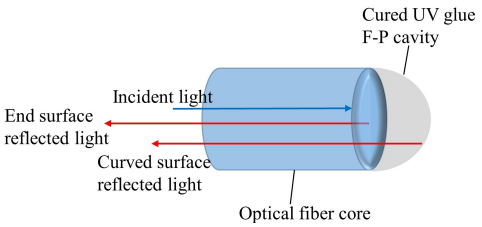

Fig. 1. Interference principle of F-P cavity.

$$\begin{cases} R_1 = (\dfrac{n_1 - n_2}{n_1 + n_2})^2 \\ R_2 = (\dfrac{n_2 - n_3}{n_2 + n_3})^2 \end{cases} \tag{1}$$

where n_1, n_2 and n_3 are the refractive index of single-mode optical fiber core, cured UV glue, and air. n_1, n_2 and n_3 are 1.46, 1.5 [21] and 1 in this paper. The calculated values of R_1 and R_2 are 0.00018 and 0.04. In practical applications, the F-P cavity only considers the interference of the first two reflected lights. Its interference principle can be derived through the double-beam interference model. The complex amplitudes of the two reflected lights [22] are:

$$\begin{cases} E_1 = E_0\sqrt{R_1} \\ E_2 = E_0(1 - R_1)(1 - \alpha)\sqrt{R_2}exp(-2j\phi) \end{cases} \tag{2}$$

where $\phi = 2\pi nL/\lambda$ is the phase difference between the two beams of light in the cavity, n is the refractive index of the cured UV glue, L is the cavity length, λ is the wavelength of the incident light, E_0 is the electric field of the incident light, α is the transmission loss in the F-P cavity. Then the reflection spectrum function [23], [24] is:

$$I = I_1 + I_2 + \cos(\varphi)\sqrt{I_1 I_2}. \tag{3}$$

$$\varphi = \frac{4\pi nL}{\lambda}. \tag{4}$$

where I_1 and I_2 are the reflected light intensities of the two end surfaces, $I_1 = R_1$, $I_2 = (1 - R_1)^2(1 - \alpha)^2 R_2$. The interference fringe free spectral range of a single F-P cavity can be expressed as [25]:

$$FSR = \lambda_m - \lambda_{m+1} \approx \frac{\lambda^2}{2nL}. \tag{5}$$

According to the working principle of the F-P cavity, the numerical simulation results of different reflection spectra can be obtained by making different cavity lengths, as shown in Fig.2. Where $\alpha = 0.4$. It can be seen from the figure that the free spectral range of the interference fringe of the F-P cavity is inversely proportional to the cavity length, which is consistent with the theoretical formula (5).

B. Temperature sensing principle

When the external temperature changes, the length and refractive index of the F-P cavity changes, the temperature response sensitivity of the sensor probe can be expressed as:

$$S_T = \frac{d\lambda}{dT} = \lambda(\frac{1}{L}\frac{dL}{dT} + \frac{1}{n}\frac{dn}{dT}). \tag{6}$$

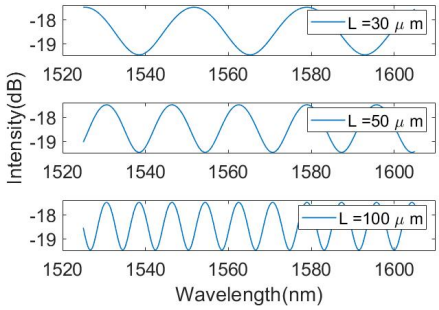

Fig. 2. Reflection spectra with different F-P cavity lengths.

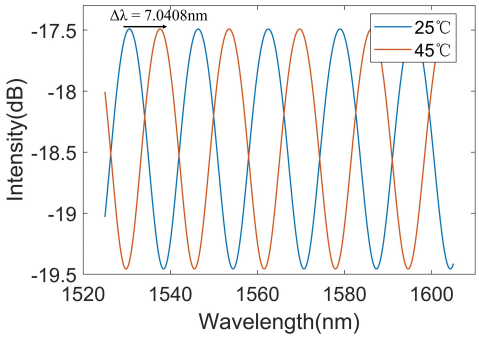

Fig. 3. Simulation of interference spectra at different temperatures.

where T is the temperature of the object to be tested. $\frac{1}{L}\frac{dL}{dT}$ and $\frac{1}{n}\frac{dn}{dT}$ are the thermal expansion coefficien (TEC) and thermo-optical coefficient (TOC) of the cured UV glue respectively. The UV glue has a relatively large thermal expansion coefficient after being cured, it is about $2.3\times10^{-4}/\,^{\circ}\mathrm{C}$ [21], which has a high sensitivity to temperature changes. It is more significant than refractive index change. Therefore, this paper mainly considers the response of the cavity length of UV glue to temperature.

When the temperature of the object changes, the optical path difference of the optical signal reflected by the fiber end face and the UV glue surface changes, resulting in a spectrum shift. External parameter values are determined by detecting the spectral shifts. To the temperature sensing principle of the F-P cavity, if the length of the F-P cavity is 50 μm, the temperature rises from the initial 25 °C to 45 °C, the F-P length is calculated to be 50.23 μm based on the thermal expansion coefficient formula. The F-P cavity reflection spectra at two temperatures are shown in Fig.3. It can be found that as the temperature increases, the cavity length increases, and the reflection spectrum is red-shifted. The numerical simulation results can calculate the temperature sensitivity to be 352.04 $pm/\,^{\circ}\mathrm{C}$. Considering the complexity of the packaging process and the sensitivity of the sensor, this article chose capillary copper tubes and cured UV glue to make the temperature-sensing probe.

C. Fabrication of Temperature Sensing Probe

This paper developed a new type of optical fiber temperature sensing probe with F-P cavity structure encapsulated in capillary copper tubes. A standard single-mode fiber with a cladding diameter of 125 um was selected, and a high-strength, highly transparent shadowless UV glue (UV3493) was coated on the end of the optical fiber and cured to form the F-P cavity. Then it was encapsulated with a capillary copper tube with an inner diameter of 0.9 mm (the same as the inner diameter of the optical fiber tight tube), a thickness of 0.2 mm, and a length of 20 mm. The F-P cavity was placed 5 mm away from the upper end surface of the copper tube, and both ends of the copper tube were cured and sealed with UV glue. Specifically, peeled off 5 cm of the coating layer at the end of fiber A, wiped it clean with alcohol, cut the end section flat with a fiber cleaver and left 2 cm, fixed the fiber with a clamp and placed it vertically, as shown in Fig.4. The other optical fiber B was also operated in the same way to obtain a flat end face. Then it was dipped in UV glue and repeatedly applied to the end of optical fiber A to ensure that a droplet shape was formed. After observing a stable interference signal using a spectrometer (YOKOGAWA AQ6370D), the end of optical fiber A was cured by ultraviolet light for 5 minutes.

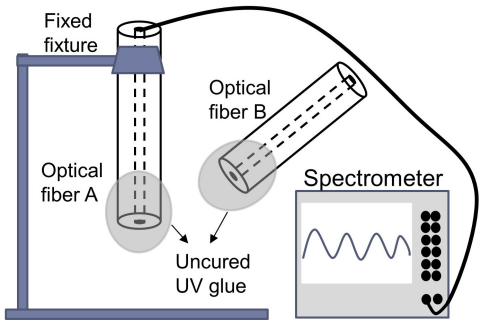

Fig. 4. The fabricating process of optical fiber temperature sensing probe.

To protect the F-P cavity and have good thermal conductivity, a capillary copper tube was selected to encapsulate it, and the interference spectrum of this temperature sensing probe was obtained by FD wavelength meter type I interrogator (Wuhan O-Optics Technology CO., LTD.). As shown in Fig.5, the lower left of the figure is sensing probe, and the right bottom is the enlarged F-P cavity structure on the display screen of the Fusion splicer. The thickness of cured UV glue at the optical fiber end is about 45.74 μm, and its refractive index is 1.5. The center wavelength of the interference spectrum is 1550 nm, and the FSR calculated from Eq. (5) is 17.21 nm. It is close to the distance (16.11 nm) between adjacent dips in the actual reflection spectrum in Fig.5.

III. Experimental Results and Discussion

To verify the long-term stability of the temperature monitoring by the sensing probe, the interference spectrum signals were analyzed on the first, tenth, and twelfth days at room temperature. We placed the optical fiber temperature sensing probe and the electronic temperature sensor (DL11B-MC, Guangzhou Dalin Electronic Technology Co., Ltd) on the experimental bench, and covered them with thermal insulation cotton to isolate them from the flowing air. Each test was conducted in a relatively stable environment for 8 minutes.

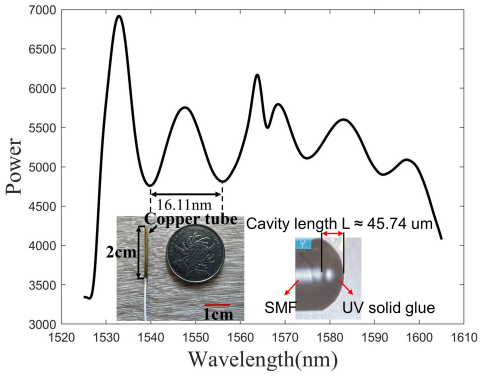

Fig. 5. Physical picture and interference spectrum of temperature sensing probe.

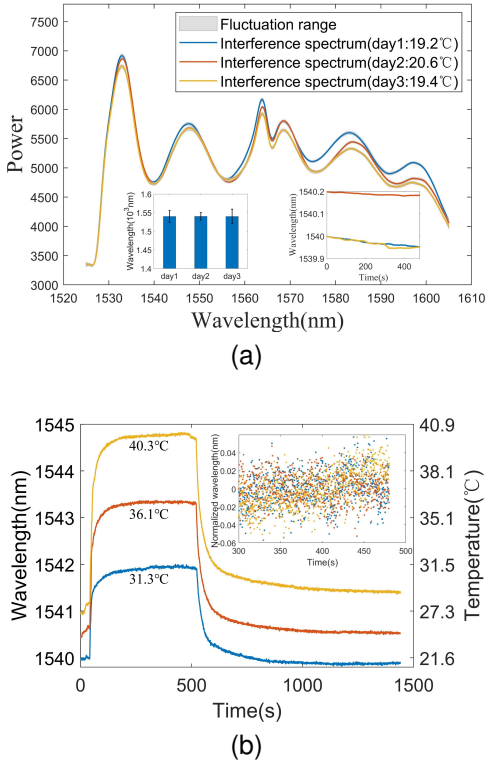

Fig. 6. Interference spectrum changes. (a) At room temperature; (b) At different constant temperatures.

Fig.6(a) shows the spectra of long-term monitoring at room temperature over the past three days. The shaded part of the curve is the fluctuation range of the spectrum during this time period. The histograms with error bars record the standard deviation of the first dip wavelength. It can be seen that at room temperature, the mean standard deviation is 16.7 pm. After the probe stayed at room temperature for 40 s, it was placed on a constant-temperature heating table at 31.3 °C, 36.1 °C, and 40.3 °C to collect 8-minute spectral data, as shown in Fig.6(b). The wavelength range fluctuated within ±60 pm after wavelength centering process. The test results show that the sensing probe has relatively good stability at different constant temperatures.

In addition, the spectral signals monitored for a long time under constant temperature conditions have a slight drift problem, as shown in the lower right of Fig.6(a). The data measured on different days have different degrees of dip wavelength blue shift over time. For the accuracy of subsequent measurements, when the probe is initially used, spectral data at room temperature are collected for self-compensation, that is:

$$\lambda_C = \lambda_T + \lambda_{Init0} - \lambda_{Init}. \tag{7}$$

Where λ_C is the compensated dip wavelength, λ_T is the temperature spectrum dip wavelength collected on the actual test object, λ_{Init} is the spectral dip wavelength value collected before use, and λ_{Init0} is the first value of λ_{Init}.

We conducted a comparison between the physical dimensions and thermal conductivity of temperature sensing probes and electronic sensors. The temperature sensing probe measures 1.3 mm by 20 mm, encased in a copper tube packaging, exhibiting a thermal conductivity of 385 $W/(mK)$. In contrast, the electronic sensor, measuring 3 mm by 30 mm, is encapsulated in standard stainless steel with a thermal conductivity ranging from 15 to 30 $W/(mK)$. These findings illustrate that capillary copper tubes offer superior heat conduction capabilities, enabling faster and more effective heat transfer than that of electronic sensors. To test the response ability of the sensing probe to temperature, the electronic sensor and the optical fiber sensing probe were collected simultaneously at room temperature for about 40 s and then placed them on a heating stage with a constant temperature of 31.3 °C. The temperature response curves of the two sensors are shown Fig.7(a). It can be found that the response speed of the F-P sensing probe is faster and reaches stability in about 2 minutes, indicating that the response of the capillary copper tube structure to temperature is more sensitive than that of the electronic sensor, and the stabilization time meets the needs of body temperature monitoring.

To test the repetitive response ability of the sensing probe to temperature, the temperature heating table was kept constant at 40.3 °C. After collecting spectral data for 30 s on the heating table, the optical fiber sensing probe was placed at room temperature for 1 minute and 30 seconds, then placed on the heating table again, and the operation was repeated three times. The temperature change curve of the F-P temperature sensing probe is shown in Fig.7(b). It can be seen that the response of the optical fiber probe to temperature has good repeatability.

To investigate the ability of temperature sensing probe to monitor human body temperature, we tested its sensitivity. The optical fiber sensing probe and electronic sensor were fixed on the aluminum substrate heating table with PI heat-resistant tape and covered with heat-insulating cotton. As shown in Fig.8(a), the heating table temperature was set from 30 °C to 45 °C with a step size of 1 °C, covering the range of human body temperature changes. Due to the slow response speed of the electronic sensor, after the temperature of the electronic sensor was initially stabilized, the current spectral data of the optical fiber sensing probe was recorded, and three days of calibration data were collected. As shown in Fig.8(b), as the

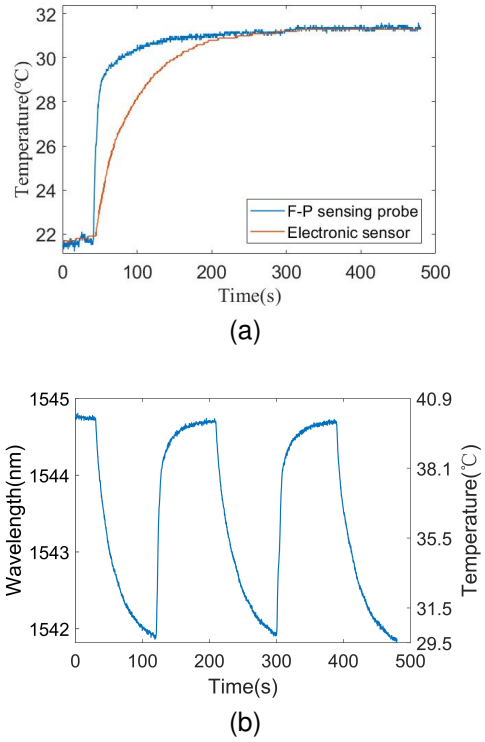

Fig. 7. F-P sensing probe temperature response. (a) Comparison of temperature response between F-P sensing probe and electronic sensor; (b) Repeated response between two temperatures.

temperature increases, the interference spectrum undergoes a red shift.

The line scan frequency of the interrogator and the temperature acquisition frequency of the electronic sensor were both set to 4 Hz. The spectral data was filtered using a sixth-order Butterworth low-pass filter with a cutoff frequency of 0.5 Hz. We performed peak-finding processing on each frame of spectral data. The preliminary dip wavelength λ_0 was obtained using the `findpeaks` function in Matlab. The wavelength range $[\lambda_0 - 3.13nm, \lambda_0 + 3.13nm]$ was truncated. Three commonly used peak fitting methods, Gaussian, Lorentz, and Polynomial fitting, were used to obtain accurate dip wavelength values, as shown in Fig.9.

The fitting formulas and results are shown in Tab.I. It can be found that the quadratic polynomial function has the best goodness of fit. Therefore, this paper chose the peak fitting method based on quadratic polynomials to obtain the dip wavelength. Finally, a scatter plot of wavelength shift with temperature was obtained, and a quadratic polynomial fitting was performed. The goodness of fit of this curve was 0.9817, and the sensitivity coefficient was approximately 287.3 $pm/°\mathrm{C}$. The sensitivity coefficient increased as the temperature increased. The F-P sensing probe designed in this article is compared with common FBG temperature sensors. When the FBG sensor is affected by the external temperature, the grating period Λ and the fiber refractive index n change. The change of the reflected light wavelength with temperature can be expressed as

$$\frac{\Delta\lambda}{\Delta T} = \lambda_B\left(\frac{1}{n}\frac{dn}{dT} + \frac{1}{\Lambda}\frac{d\Lambda}{dT}\right) = \lambda_B(\xi + \alpha). \tag{8}$$

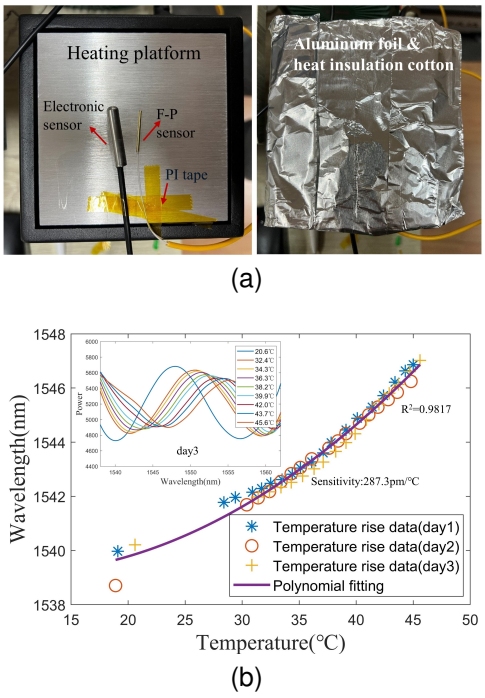

Fig. 8. Sensitivity of F-P temperature sensing probe. (a) Temperature calibration platform. (b) Temperature-wavelength fitting curve of F-P temperature sensing probe.

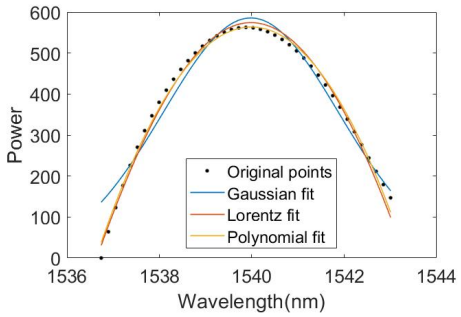

Fig. 9. Comparison of three different peak fitting algorithms.

where ξ is the thermo-optical coefficient that affects the refractive index of the fiber, and α is the thermal expansion coefficient that affects the grating period. Different FBG sensing materials or packaging materials have different properties. As shown in Tab.II, Materials with a high thermal expansion coefficient or thermo-optical coefficient can significantly improve the sensitivity of the optical fiber temperature sensor. This has important reference significance for the selection of optical fiber manufacturing or packaging materials, which can meet the requirements for measurement temperature and sensitivity in different application scenarios.

Since the optical fiber temperature sensing probe output spectral signal is red-shifted with temperature, we use the SNR to quantify the degree to which the wavelength shift stands out from the noise. The amplitude of the signal can be defined as the change in wavelength $\Delta\lambda$ as the temperature changes. The noise level is estimated using the standard deviation σ of the dip wavelength at constant temperature. The SNR can be

TABLE I
FITTING METHODS AND RESULTS

Methods	Parameters	Goodness of fit
Gaussian fit: $f(x) = a_1 \cdot exp(-(\frac{(x-b_1)}{c_1})^2)$	$a_1 = 585.5495$ $b_1 = 1539.9793(\lambda_{dip})$ $c_1 = 2.6819$	0.9522
Lorentz fit: $f(x) = \frac{a}{(x-b)^2+c} + d$	$a = 1.1807 \times 10^6$ $b = 1539.9847(\lambda_{dip})$ $c = 146.0108$ $d = -7.5121 \times 10^3$	0.9891
Polynomial fit: $f(x) = p_1 \cdot x^2 + p_2 \cdot x + p_3$	$p_1 = -49.7893 \times 10^6$ $p_2 = 1.5335 \times 10^5$ $p_3 = -1.1808 \times 10^8$ $\lambda_{dip} = 1.539.9904$	**0.9927**

TABLE II
COMPARISON OF OPTICAL FIBER SENSING PERFORMANCE WITH DIFFERENT FABRICATION OR PACKAGING MATERIALS

Sensors	TOC (1/°C)	TEC (1/°C)	Sensitivity (pm/°C)
SMF28-FBG [26]	0.55 × 10^{-6}	12.9 × 10^{-6}	8–11
FBG(PLA encapsulated) [15]	4.1 × 10^{-5}	–	139
CYTOP-FBG(TPU encapsulated) [27]	2.0 × 10^{-5}	–	30.8
PMMA-FBG [28]	(70-77)×10^{-6}	-1×10^{-4}	-131.1±4.9
F-P Probe	2.3×10^{-4}	–	**287.3**

calculated by the formula (9). The average standard deviation measured at constant room temperature for three days was 16.7 pm, and the signal-to-noise ratio under a temperature change of 20°C was 50.7 dB

$$SNR = 20lg(\frac{\Delta\lambda}{\sigma}). \tag{9}$$

During the rehabilitation training process of the subject, the body surface temperature of the training part will change with the amount of training tasks. The assistance rehabilitation equipment can regulate the training tasks by monitoring the body surface temperature to achieve the purpose of intelligent rehabilitation training. The monitoring of armpit temperature can reflect a person's true body temperature. Based on the relationship between body temperature and metabolism in rehabilitation training, it can evaluate the energy consumption and fatigue level of the trainer and provide feedback for the customization of intelligent rehabilitation programs. Therefore, to study the feasibility of monitoring human body temperature with optical fiber sensing probe, the sensing probe was placed on the human wrist and armpit to achieve the monitoring capability of local body surface and real body temperature. This trial has been approved by Human Participants Ethics Committee from Wuhan University of Technology, and written informed consent was obtained from each participant. When measuring the body surface temperature, the probe was kept at room temperature (17.8 °C) for 30 s, and then affixed to the wrist with K-Tape (Kinesio Tape). Using medical tape to attach sensors to the human body is a common practice in

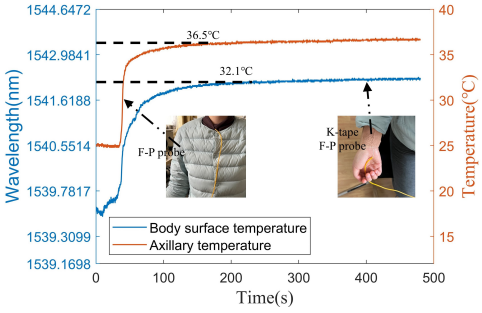

Fig. 10. Body temperature measurement curve.

medical and research environments [29].They provide a non-invasive, flexible, convenient and adjustable wearing solution. As shown in Fig.10. The F-P sensing probe reached a stable value of 32.1 °C in three and a half minutes, which is in line with the human body surface temperature range of 32 - 35 °C [30]. When measuring armpit temperature, the F-P sensing probe was kept at room temperature (24.6 °C) for 40 s and then placed it under the armpit. It reached a stable value of 36.5 °C in about 2 and a half minutes, which is consistent with the armpit temperature range of 35.3 - 37 °C [31]. The experimental results verify the feasibility of our proposed F-P temperature sensing probe that can quickly sense temperature changes and measure the body temperature of different parts of the human body.

Although the current work has verified the effectiveness of the sensing probe in measuring body temperature, there are still some shortcomings. The F-P probe is fixed using medical tape. Although the fixation is relatively simple and stable, sticking and tearing it off will still cause some discomfort. In the future, we will consider fixing the sensing probe into flexible Velcro straps or vest fabric to facilitate body temperature monitoring during daily activities for longer periods of time. In addition, common standard temperature calibration sources include thermocouples, platinum resistors, and constant temperature chambers. Currently, thermocouple electronic sensors are used as the calibration source for this article, which can continuously monitor and facilitate data export. Although the measurement resolution is 0.1 °C, the measurement accuracy is 0.5 °C, which is lower than national standard requirements for electronic thermometers. At the same time, due to the difference in response speed and stability between calibration source and the F-P fiber optic sensing probe, there will also be a certain error in the calibration curve. In the future, calibration source with higher accuracy and stability will be considered.

IV. CONCLUSION

This paper develops an optical fiber temperature sensing probe based on F-P cavity, which has the characteristics of simple packaging, fast response speed, high sensitivity, good repeatability, and high SNR. The sensing probe can not only accurately monitor the surface and core temperature of the human body, but also supports multi-point distributed measurement, thereby effectively capturing detailed information

of the human body temperature field. In addition, integrating F-P sensing with multi-modal optical fiber sensors can expand the application scope of the sensing system and can monitor physiological parameters such as respiration, heart rate, and body surface humidity, as well as motion parameters such as angle and muscle deformation. This multi-modal sensor system is not only capable of effectively and accurately predicting the user's steady-state metabolism, but also demonstrates the potential to achieve feedback on the human body's intentions and optimize rehabilitation strategies by collecting and analyzing human physiological and movement signals.

REFERENCES

[1] U. Nations, "World population prospects 2022," [Online], 2022.7.11, Available: https://population.un.org/wpp/.

[2] B. Chen, H. Ma, L.-Y. Qin, F. Gao, K.-M. Chan, S.-W. Law, L. Qin, and W.-H. Liao, "Recent developments and challenges of lower extremity exoskeletons," *Journal of Orthopaedic Translation*, vol. 5, pp. 26–37, 2016. [Online]. Available: https://www.sciencedirect.com/science/article/pii/S2214031X15000716

[3] M. Behrens, M. Gube, H. Chaabene, O. Prieske, A. Zenon, K.-C. Broscheid, L. Schega, F. Husmann, and M. Weippert, "Fatigue and human performance: An updated framework," *Sports Medicine*, vol. 53, no. 1, pp. 7–31, 2023. [Online]. Available: https://doi.org/10.1007/s40279-022-01748-2

[4] K. T, G. K. Rajini, and D. Maji, "Cost-effective, disposable, flexible, and printable mwcnt-based wearable sensor for human body temperature monitoring," *IEEE Sensors Journal*, vol. 22, no. 17, pp. 16 756–16 763, 2022.

[5] W. A. Altabey, Z. Wu, M. Noori, and H. Fathnejat, "Structural health monitoring of composite pipelines utilizing fiber optic sensors and an ai-based algorithm—a comprehensive numerical study," *Sensors*, vol. 23, no. 8, 2023.

[6] W. Liu, C. Liu, J. Wang, J. Lv, Y. Lv, L. Yang, N. An, Z. Yi, Q. Liu, and C. Hu, "Surface plasmon resonance sensor composed of microstructured optical fibers for monitoring of external and internal environments in biological and environmental sensing," *Results in Physics*, vol. 47, p. 106365, 2023.

[7] G. A. Wellbrock, T. J. Xia, M. F. Huang, S. Han, Y. Chen, T. Wang, and Y. Aono, "Explore benefits of distributed fiber optic sensing for optical network service providers," *Journal of Lightwave Technology*, vol. 41, no. 12, pp. 3758–3766, 2023.

[8] X. Zhang, C. Wang, T. Zheng, H. Wu, Q. Wu, and Y. Wang, "Wearable optical fiber sensors in medical monitoring applications: A review," *Sensors*, vol. 23, no. 15, p. 6671, 2023.

[9] Z. Wang, Z. Chen, L. Ma, Q. Wang, H. Wang, A. Leal-Junior, X. Li, C. Marques, and R. Min, "Optical microfiber intelligent sensor: Wearable cardiorespiratory and behavior monitoring with a flexible wave-shaped polymer optical microfiber," *ACS Appl Mater Interfaces*, vol. 16, no. 7, pp. 8333–8345, 2024. [Online]. Available: https://www.ncbi.nlm.nih.gov/pubmed/38321958

[10] T. Li, Y. Su, F. Chen, H. Zheng, W. Meng, Z. Liu, Q. Ai, Q. Liu, Y. Tan, and Z. Zhou, "Bioinspired stretchable fiber-based sensor toward intelligent human–machine interactions," *ACS Applied Materials Interfaces*, vol. 14, no. 19, pp. 22 666–22 677, 2022.

[11] A. G. Leal-Junior, A. Frizera, L. Vargas-Valencia, W. M. dos Santos, A. P. L. Bo, A. A. G. Siqueira, and M. J. Pontes, "Polymer optical fiber sensors in wearable devices: Toward novel instrumentation approaches for gait assistance devices," *IEEE Sensors Journal*, vol. 18, no. 17, pp. 7085–7092, 2018.

[12] N. Peng, W. Meng, Q. Wei, Q. Ai, Q. Liu, and S. Xie, "Wearable optical fiber sensors for biomechanical measurement in medical rehabilitation: A review," *IEEE Sensors Journal*, vol. 23, no. 12, pp. 12 455–12 469, 2023.

[13] J. Moreno, L. Bueno, J. L. Pons, J. Baydal-Bertomeu, J. Belda-Lois, J. Prat, and R. Barberá, "Wearable robot technologies," in *Wearable robots: biomechatronic exoskeletons*. Hoboken: John Wiley & Sons, 2008, pp. 165–199.

[14] M. Li and Y. Liao, *Fiber optic sensors technology*. Wuhan: Wuhan University Press, 2012.

[15] A. Leal-Junior, J. Casas, C. Marques, M. Pontes, and A. Frizera, "Application of additive layer manufacturing technique on the development of high sensitive fiber bragg grating temperature sensors," *Sensors*, vol. 18, no. 12, p. 4120, 2018.

[16] A. Leal-Junior, A. Frizera-Neto, C. Marques, and M. J. Pontes, "Measurement of temperature and relative humidity with polymer optical fiber sensors based on the induced stress-optic effect," *Sensors*, vol. 18, no. 3, p. 916, 2018. [Online]. Available: https://www.ncbi.nlm.nih.gov/pubmed/29558387

[17] Y. Liu, D. Yang, Y. Wang, T. Zhang, M. Shao, D. Yu, H. Fu, and Z. Jia, "Fabrication of dual-parameter fiber-optic sensor by cascading FBG with FPI for simultaneous measurement of temperature and gas pressure," *Optics Communications*, vol. 443, pp. 166–171, 2019.

[18] Y. Wang, Q. Huang, W. Zhu, and M. Yang, "Simultaneous measurement of temperature and relative humidity based on FBG and FP interferometer," *IEEE Photonics Technology Letters*, vol. 30, no. 9, pp. 833–836, 2018.

[19] H. R. Chowdhury and M. Han, "Fiber optic temperature sensor system using air-filled Fabry-Perot cavity with variable pressure," *Sensors*, vol. 23, no. 6, 2023.

[20] J. Liang, J. Qu, J. Ye, Y. Liu, and S. Qu, "Ultra-sensitive temperature sensor of cascaded dual PDMS-cavity based on enhanced vernier effect," *IEEE Sensors Journal*, vol. 23, no. 3, pp. 2264–2269, 2023.

[21] G. Zhang, M. Yang, and M. Wang, "Large temperature sensitivity of fiber-optic extrinsic fabry–perot interferometer based on polymer-filled glass capillary," *Optical Fiber Technology*, vol. 19, no. 6, pp. 618–622, 2013.

[22] E. Hecht, *Optics*. Pearson Education India, 2012.

[23] M. Deng, C. P. Tang, T. Zhu, and Y. J. Rao, "PCF-based Fabry–Pérot interferometric sensor for strain measurement at high temperatures," *IEEE Photonics Technology Letters*, vol. 23, no. 11, pp. 700–702, 2011.

[24] B. H. Lee, Y. H. Kim, K. S. Park, J. B. Eom, M. J. Kim, B. S. Rho, and H. Y. Choi, "Interferometric fiber optic sensors," *Sensors*, vol. 12, no. 3, pp. 2467–2486, 2012.

[25] S. C. Warren-Smith, R. M. André, J. Dellith, T. Eschrich, M. Becker, and H. Bartelt, "Sensing with ultra-short Fabry-Perot cavities written into optical micro-fibers," *Sensors Actuators B: Chemical*, vol. 244, pp. 1016–1021, 2017.

[26] T. Toyoda and M. Yabe, "The temperature dependence of the refractive indices of fused silica and crystal quartz," *Journal of Physics D: Applied Physics*, vol. 16, no. 5, p. L97, 1983.

[27] A. Leal-Junior, A. Theodosiou, C. Diaz, C. Marques, M. J. Pontes, K. Kalli, and A. Frizera-Neto, "Fiber bragg gratings in cytop fibers embedded in a 3d-printed flexible support for assessment of human-robot interaction forces," *Materials*, vol. 11, no. 11, p. 2305, 2018.

[28] C. A. F. Marques, P. Antunes, P. Mergo, D. J. Webb, and P. Andre, "Chirped bragg gratings in pmma step-index polymer optical fiber," *IEEE Photonics Technology Letters*, vol. 29, no. 6, pp. 500–503, 2017.

[29] X. He, W. Wang, S. Yang, F. Zhang, Z. Gu, B. Dai, T. Xu, Y. Y. S. Huang, and X. Zhang, "Adhesive tapes: From daily necessities to flexible smart electronics," *Applied Physics Reviews*, vol. 10, no. 1, 2023.

[30] R. A. Freitas, *Nanomedicine, volume I: basic capabilities*. Landes Bioscience Georgetown, TX, 1999, vol. 1.

[31] M. Sund-Levander, C. Forsberg, and L. K. Wahren, "Normal oral, rectal, tympanic and axillary body temperature in adult men and women: A systematic literature review," *Scandinavian journal of caring sciences*, vol. 16, no. 2, pp. 122–128, 2002.